

Evidence of Magnetic Helicity in Emerging Flux and Associated Flare

R. Chandra · B. Schmieder · G. Aulanier · J.M. Malherbe

Received: 18 July 2008 / Accepted: 2 June 2009 / Published online: 26 June 2009
© Springer Science+Business Media B.V. 2009

Abstract The aim of this paper is to look at the magnetic helicity structure of an emerging active region and show that both emergence and flaring signatures are consistent with a same sign for magnetic helicity. We present a multiwavelength analysis of an M1.6 flare occurring in the NOAA active region 10365 on 27 May 2003, in which a large new bipole emerges in a decaying active region. The diverging flow pattern and the “tongue” shape of the magnetic field in the photosphere with elongated polarities are highly suggestive of the emergence of a twisted flux tube. The orientation of these tongues indicates the emergence of a flux tube with a right-hand twist (*i.e.*, positive magnetic helicity). The flare signatures in the chromosphere are ribbons observed in H α by the MSDP spectrograph in the Meudon solar tower and in 1600 Å by TRACE. These ribbons have a J shape and are shifted along the inversion line. The pattern of these ribbons suggests that the flare was triggered by magnetic reconnection at coronal heights below a twisted flux tube of positive helicity, corresponding to that of the observed emergence. It is the first time that such a consistency between the signatures of the emerging flux through the photosphere and flare ribbons has been clearly identified in observations. Another type of ribbons observed during the flare at the periphery of the active region by the MSDP and SOHO/EIT is related to the existence of a null point, which is found high in the corona in a potential field extrapolation. We discuss the interpretation of these secondary brightenings in terms of the “breakout” model and in terms of plasma compression/heating within large-scale separatrices.

R. Chandra (✉) · B. Schmieder · G. Aulanier · J.M. Malherbe
Observatoire de Paris, LESIA, UMR8109 (CNRS), 92195 Meudon Principal Cedex, France
e-mail: chandra.ramesh@obspm.fr

B. Schmieder
e-mail: brigitte.schmieder@obspm.fr

G. Aulanier
e-mail: guillaume.aulanier@obspm.fr

J.M. Malherbe
e-mail: jean-marie.malherbe@obspm.fr

R. Chandra
Uttarakhand Department of Science and Technology, C/O Office of the District Magistrate, Nainital,
India

Keywords Flares · Magnetic reconnection · Helicity · Magnetic field

1. Introduction

It is believed that flare energy originates from the free energy stored in nonpotential magnetic structures. Magnetic reconnection is considered to play an important role in the sudden release of energy in solar flares. Several conditions – such as flux emergence, high magnetic field gradient, and flux cancellation – are commonly found near flare locations.

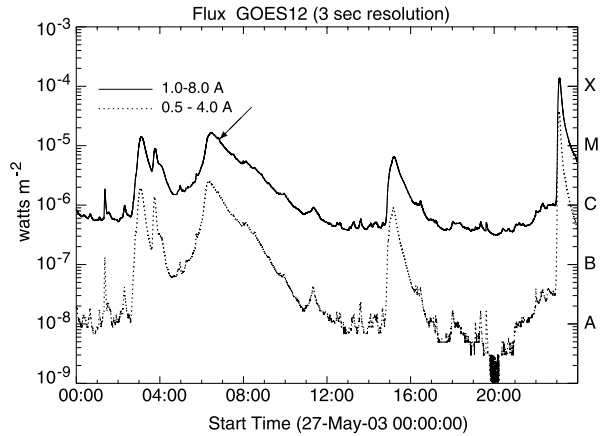
Magnetic complexity plays an important role in strong solar activity, as studied by many authors (*i.e.*, Schmieder and van Driel-Gesztelyi, 2005; Sammis, Tang, and Zirin, 2000; Antiochos, DeVore, and Klimchuk, 1999). The magnetic complexity is commonly due to slow or fast evolution of the magnetic configuration. Shear and flux emergence are responsible for such changes in the magnetic field. Hagyard, Venkatakrishnan, and Smith (1990) have shown that the magnetic field in flaring locations is strongly sheared. Large-scale shear in the magnetic field can be built up through the slow motion of footpoints stretching the length of loops. This evolution can progress through stable field configurations (Roudier *et al.*, 2008). However, magnetic shear alone is not a sufficient condition. Flux emergence has long been considered as an important condition to trigger solar flares (Heyvaerts, Priest, and Rust, 1977; Martin *et al.*, 1982; Shibata, Nozawa, and Matsumoto, 1992; Schmieder *et al.*, 1994; Choudhary, Ambastha, and Ai, 1998; Chen and Shibata, 2000; Zhang, Zhang, and Zhang, 2008; and references therein). A new magnetic flux tube emerges from below the photosphere and interacts with the pre-existing flux tubes. Reconnection occurs in the current sheet, which forms between the old and new fluxes (Heyvaerts, Priest, and Rust, 1977). The magnetic flux may emerge already twisted (Leka *et al.*, 1996). Subphotospheric motions are the drivers of free energy storage and the emerging flux provides the trigger mechanism for impulsive energy release (Zhao and Kosovichev, 2004; Mason *et al.*, 2006).

Magnetic helicity is a parameter indicating the degree of twist and writhe in an active region (see the reviews by Démoulin, 2007; Démoulin and Pariat, 2009). The helicity pattern of the Sun has characteristic features governed by a hemispheric rule, with positive (negative) magnetic helicity being common in the south (north) hemisphere. Pevtsov (2002) summarized the different possible signatures of magnetic helicity observed on the Sun: sunspot whorls, filament chirality, sigmoids, and flare ribbons. Appearance of magnetic “tongues” in an emerging active region as first discussed by López Fuentes *et al.* (2000) is an important signature, revealing information on the helicity sign of the active region. We will use these proxies to derive the magnetic helicity of our active region. Sometimes there are mixed magnetic helicity zones in the active region. Therefore it is not always necessary for the helicity sign to be the same in all the observational features (Green *et al.*, 2007; Chandra *et al.*, 2009).

The analysis of magnetic topology of an active region gives us information on possible locations of magnetic reconnection: null points (locations where magnetic field vanishes), separatrices (which separate different connectivity domains), quasi-separatrix layers (QSLs) (regions where there is a drastic change in field line linkage). QSLs are a generalization of the concept proposed by Priest and Démoulin (1995) and applied to the modeling of J-shaped two-ribbon flares by Démoulin, Priest, and Lonie (1996).

In this paper, we study the evolution and magnetic configuration of the M1.6 flare that occurred in NOAA active region (AR) 10365 on 27 May 2003, using multiwavelength observations. We present the instrumentation and observations in Section 2. Section 3 describes the evolution of the magnetic field in the active region. The description of the flare at different wavelengths is presented in Section 4. In Section 5 we explain the relationship between the magnetic helicity of the twisted emerging flux tube and the magnetic reconnection leading to the M1.6 flare with J-shaped main ribbons. In Section 6, we show the results of a

Figure 1 Temporal evolution of the flare in GOES 12 X rays at 0.5–4 Å and 1–8 Å on 27 May 2003. The studied M1.6 flare is shown by an arrow.



linear force-free field (lfff) model of the large-scale active region configuration and provide an interpretation for the presence of semicircular brightenings (secondary ribbons) in its periphery. We finally conclude that it is the first time that signatures of magnetic helicity in the photosphere (presence of tongues in longitudinal magnetic field maps), in the chromosphere (J-shaped ribbons), and in the corona (hard X-ray sources) are shown in combination and found to be consistent.

2. Instrumentation and Observations

The M1.6 flare occurring in NOAA AR 10365 located S08°W10° on 27 May 2003 was the target of an international campaign. This flare is associated with a coronal mass ejection (CME) observed by the Large Angle Spectroscopic Coronagraph (LASCO; Brueckner *et al.*, 1995) at 06:50 UT. The complex morphology of the ribbons observed at the Meudon solar tower was intriguing and initiated this study.

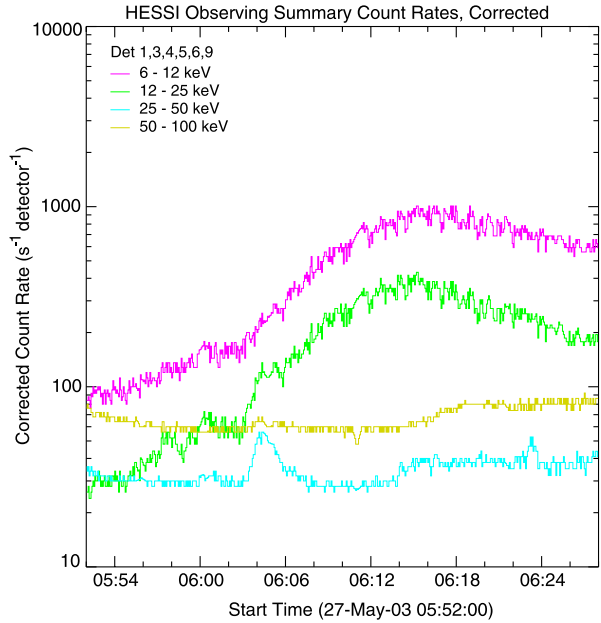
Figure 1 shows the temporal evolution of the flare observed by GOES 12. The eruption onset starts at 05:40 UT with a flux of $3.5 \times 10^{-6} \text{ W m}^{-2}$. The maximum flux is reached around 06:15 UT with a value in X rays (1–8 Å) of $1.6 \times 10^{-5} \text{ W m}^{-2}$. This is a long-duration event that ended around 10:00 UT.

Figure 2 presents the temporal evolution of the flare in hard X rays (HXR) observed by the Reuven Ramaty High-Energy Solar Spectroscopic Imager (RHESSI). The time profiles show that the X-ray emissions above 25 keV are very low. The time profiles indicate that the thermal component is dominant in the flare. The two low-energy band emissions slightly increase after 05:40 UT until 06:15 UT, with an impulsive event at 06:04 UT detectable in the higher energy band (25–50 keV).

In this study, we use data from the *Solar and Heliospheric Observatory* Michelson Doppler Imager (SOHO/MDI) (with a time cadence of 96 minutes and a pixel size of 1.98''; Scherrer *et al.*, 1995) and EIT (with a time cadence of 12 minutes to 6 hours and a pixel size of 2.5''; Delaboudinière *et al.*, 1995), from the *Transition Region and Coronal Explorer* (TRACE) 1600 Å (with a time cadence of 6 minutes and a pixel size of 0.5'', Handy *et al.*, 1999); and from RHESSI (Lin *et al.*, 2002) as well as the Multi channel Subtractive Double Pass spectrograph (MSDP) of the Meudon solar tower.

The M1.6 flare has been observed in the H α line (6563 Å) with the MSDP. The entrance slit of the spectrograph covers an elementary field of view of 72'' \times 465'' with a pixel size

Figure 2 Temporal evolution of the flare in HXR observed by RHESSI at 6–12, 12–15, 25–50, and 50–100 keV, respectively.



of $0.5''$. The final field of view of the images is $295'' \times 460''$. The exposure time is 40 ms. We obtained consecutive sequences of five images with a cadence of 1 minute. Using the MSDP technique (Mein, 1977, 1991) the field of view is recorded simultaneously in nine different wavelength intervals around $H\alpha$ line center, separated by 0.3 \AA . Interpolating with spline functions the observed intensity in these images, we are able to construct $H\alpha$ profiles in each point of the observed field of view. A mean or the reference disk profile is obtained by averaging over a quiet region on the disk (flat-field sequence).

3. Evolution of the Photospheric Magnetic Configuration

3.1. Global Pattern of the Emerging Flux

To understand the cause of the flare, we need to study the magnetic configuration of the active region. Using MDI magnetograms we were able to follow its evolution during several days in May of 2003 (Figure 3). On 24 May, this region had a weak-field bipolar configuration with a leading negative polarity and a diffuse following positive polarity. This corresponds to a decaying active region.

The emergence of a new bipole with a high-intensity field occurred between 24 and 25 May and was well visible inside the positive-polarity area in the magnetograms of 25 May; the bipole had a north–south orientation (with negative polarity in the north and positive polarity in the south). Because of this continuous emergence of flux in the north part of the active region, the magnitude of the positive field increased; this positive region progressively surrounded the new emergent negative flux, creating a δ -spot configuration. The active region polarities rotated anticlockwise. The rotation of the magnetic inversion line from 25 to 27 May was measured as 25° . To draw the magnetic inversion line on the SOHO/MDI magnetograms, we plot the simplified contour of zero magnetic field strength. Afterward,

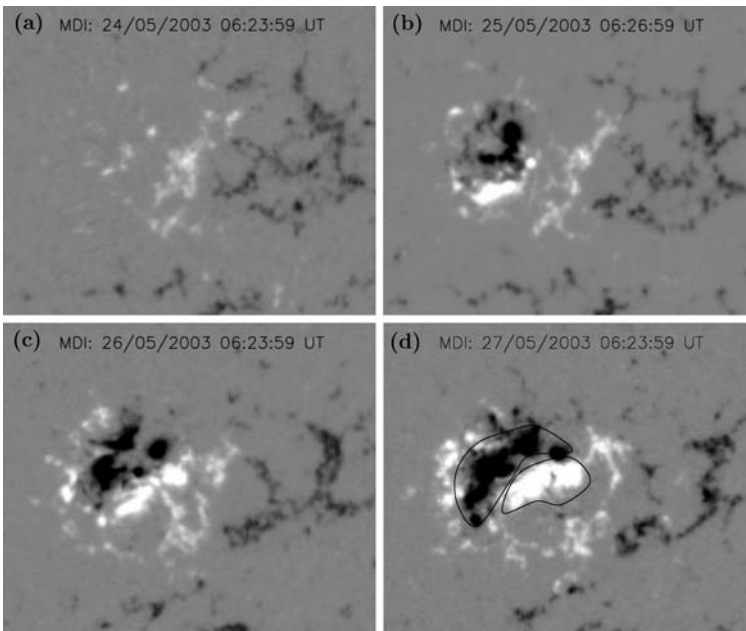


Figure 3 Evolution of the magnetic field of NOAA AR 10365. Magnetograms from 24 May 2003 to 27 May 2003 show the emergence of high-intensity flux. The contour over the magnetogram of 27 May 2003 shows the two magnetic tongues. The field of view of the images is $300'' \times 250''$. North is up and west is to the right.

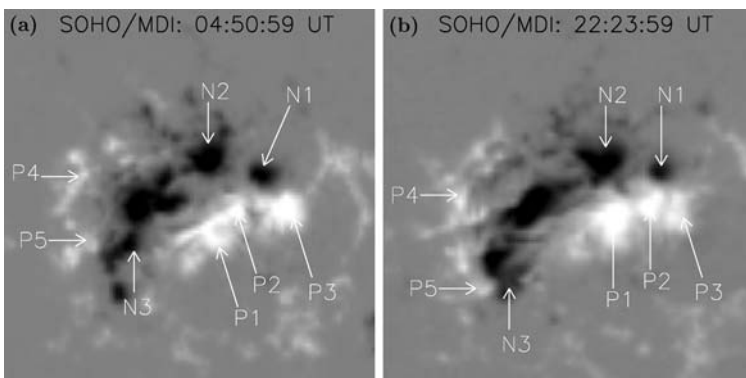


Figure 4 SOHO/MDI magnetogram of the active on 27 May 2003 at two selected times. The polarities associated with the motions described in the text are shown by arrows (P1, P2, P3, P4, P5: positive polarity; N1, N2, N3: negative polarity). The field of view of the images is $160'' \times 160''$. North is up and west is to the right.

we measure the change in angle of the magnetic inversion line between 25 May 2003 (06:26 UT) and 27 May 2003 (06:23 UT).

The emergence of the new magnetic flux is a long-term process. Looking at Figure 3, between 25 and 27 May, we see that the longitudinal magnetic field pattern of the emerging bipole is characterized by the existence of two elongated areas of opposite polarity labeled

Table 1 Movements of selected positive (P) and negative (N) polarities.

Sunspot	Direction	Velocity (km s ⁻¹)
P1	Northwest	0.18
P2	Northwest	0.18
P3	Northwest	0.07
P4	Northwest	0.14
P5	South	0.24
N1	West	0.12
N2	West	0.10
N3	South	0.22

N1, N2, and N3 (negative polarities) and P1, P2, and P3 (positive polarities). These two areas are shifted from one another along the inversion line [Figure 5(a)]. This typical pattern can be explained as follows. The series of magnetograms shows the classical appearance of a bipole followed by the separation of the two opposite magnetic polarities as observed for the emergence of a twisted Ω loop [Figure 5(b)]. An asymmetry appears in the magnetogram during the emergence of the apex of the loop because of the contribution of the azimuthal component of the emerging twisted flux tube to the observed vertical component of the photospheric field. This azimuthal component produces two elongated polarities – so-called tongues. The extension of these tongues is directly proportional to the magnitude of the twist and their position depends on the sign (positive twist in our case). The tongues are present only when the apex of the flux tube is crossing the photosphere during flux emergence. The positive (negative) polarity is elongated toward the west (east) with tongues. This pattern is a characteristic feature of a long-term twisted emerging flux tube as first described by López Fuentes *et al.* (2000) (see their Figure 5).

According to the geometry of the tongues, we conclude that the emerging flux tube has a right-hand twist corresponding to positive magnetic helicity (López Fuentes *et al.*, 2000).

3.2. Flow Pattern of the Polarities

We measure the speed of some selected positive (P1–P5) and negative (N1–N3) spots, which show large displacements (Figure 4). For the measurement of the location of the magnetic polarities on magnetograms we manually track the center of each polarity. Based on the magnetograms at 04:50 UT and at 22:23 UT on 27 May, we calculate the velocity and direction of the selected spots and report them in Table 1. From these measurements we see that the positive polarities P1, P2, P3, and P4 are moving toward the northwest, while polarity P5 is moving toward the south. The negative-polarity spots (*i.e.*, N1 and N2) are moving toward the west, while the spot N3 is going south. The velocities of these spots range from 0.07 to 0.24 km s⁻¹.

These velocities are in agreement with the local correlation tracking (LCT) analysis done by Chae, Moon, and Park (2004). The photospheric motions of these emerging spots lead to a large diverging and shearing flow pattern of the magnetic field, inducing a nonpotential configuration along the magnetic inversion line. The resulting magnetic shear plays an important role in the onset of the flare.

Figure 5 Sketch of the signatures of positive magnetic helicity observed in the NOAA AR 10365 during the M1.6 flare on 27 May 2003.

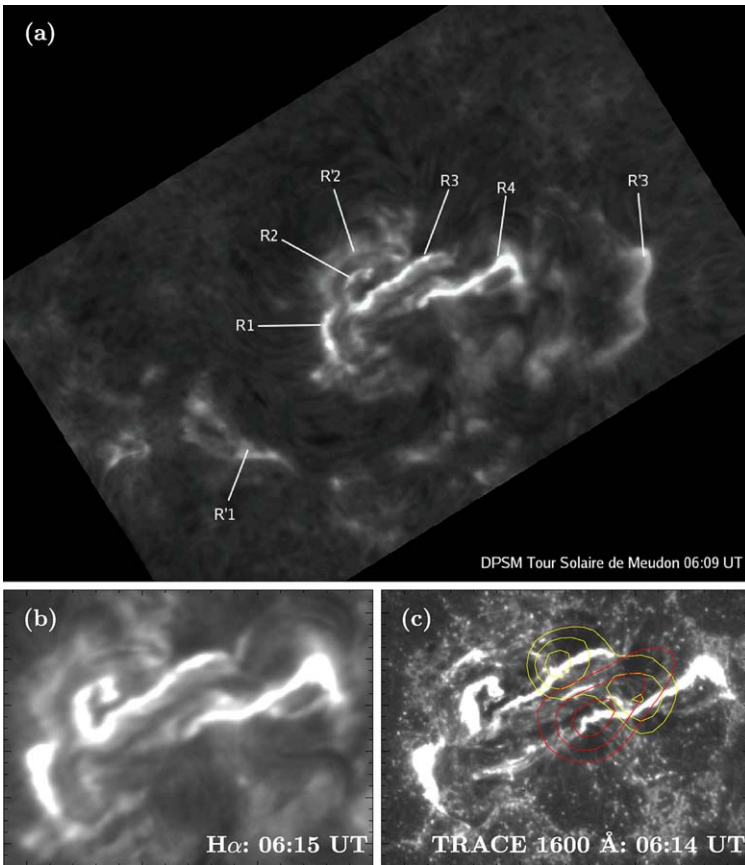
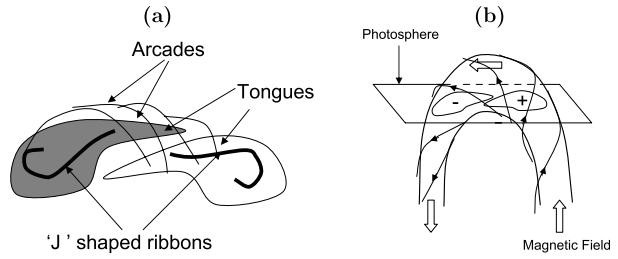


Figure 6 (a) H α line-center images of the flare observed with the MSDP spectrograph of Meudon solar tower at 06:09 UT (field of view = $456'' \times 290''$) and enlarged view of J-shaped ribbons in (b) H α line center and (c) TRACE (1600 \AA) (field of view = $160'' \times 120''$). The TRACE 1600 \AA image is overlaid by RHESSI contours (red contour: 6–12 keV and yellow contour: 25–50 keV; contour levels: 50%, 70%, and 90% of the peak intensity) at 06:04 UT. North is up and west is to the right.

4. Description of the Flare

The flare was observed in $H\alpha$ and in 1600 \AA by TRACE, presenting J-shaped ribbons in the central part of the active region and secondary arc-shaped brightenings at the periphery of the active region, as described in Section 6.

4.1. Main J-Shaped Ribbons

The flare was observed between 06:09 and 06:52 UT in $H\alpha$ with the MSDP in the solar tower of Meudon. We follow the evolution of the chromospheric ribbons in $H\alpha$. In Figure 6 we show the $H\alpha$ reconstructed images in the line center, indicating the different flare ribbons. The two main flare ribbons are J shaped. We distinguish four very bright ribbons (R1 to R4) and three dimmer secondary ribbons (R'1 to R'3). R2 and R3 are parts of the same ribbon though not formed exactly at the same time. The pairs of ribbons R1, R2 and R3, R4 are part of the main flare; they are located nonsymmetrically at both sides of the inversion line. At 06:15 UT, the peak time of the flaring event, some brightenings propagated along the flare ribbons. Such a propagation has been noticed in previous flares (Berlicki *et al.*, 2004) and may be explained by a slipping reconnection mechanism (Aulanier *et al.*, 2007).

TRACE observed the central part of the flare in 1600 \AA with a cadence of 6 minutes. This allows us to identify the central J-shaped ribbons, which were very similar to those seen in $H\alpha$. An enlarged view of the two J-shaped ribbons seen in $H\alpha$ and TRACE 1600 \AA is presented in Figures 6(b) and 6(c). We shall discuss the J-shaped ribbons in the context of emerging twisted flux in Section 5.

4.2. RHESSI Images and Spatial Correlation of $H\alpha$, TRACE, and HXR Sources

In this section we present the RHESSI images and the co-alignment of $H\alpha$, RHESSI, and TRACE 1600 \AA sources and the MDI magnetogram.

The co-alignment of RHESSI and MDI data was done by referring the relative position of the solar disk center of each field of view. As for the $H\alpha$ and TRACE (1600 \AA) data, we compare these images with white-light images of SOHO/MDI.

We reconstructed RHESSI images in 6–12, 15–20, and 25–50 keV energy channels from collimators (4F to 9F) using the CLEAN algorithm (Hurford *et al.*, 2002), which gives a spatial resolution of about 12 arcsec. The locations of RHESSI HXR sources in 6–12 and 25–50 keV overlaid on TRACE 1600 \AA are shown in Figure 6(b).

At 06:04 UT RHESSI observed two nonthermal X-ray footpoint sources in the 25–50 keV energy band, located over the main J-shaped ribbons anchored in the positive and negative polarities [cf. Figure 6(b) and Figure 7]. The 6–12 keV source corresponds to a loop-top source, which looks shifted toward the south. This may be due to projection effects. During the flare peak time (06:15 UT) RHESSI also observed two HXR sources (15–20 keV), one located at the same place as one of the previous sources (and thus it could be a recurrent phenomenon) and the other located in the east part of the region. The new source on the left was related to the brightening of ribbons R1 and R2 at 06:15 UT.

There are several different models for the acceleration of the nonthermal electrons responsible for HXR emission in the 25–50 keV range. The reconnection mechanism is commonly proposed. Other models include an electric field being generated in a reconnection region or in shocks or turbulence. Following acceleration, electrons precipitate along the magnetic field to denser layers of the atmosphere. Electron energy loss in the chromosphere from Coulomb collisions leads to heating, causing evaporation along the loops, whereas electron-ion bremsstrahlung leads to HXR emission.

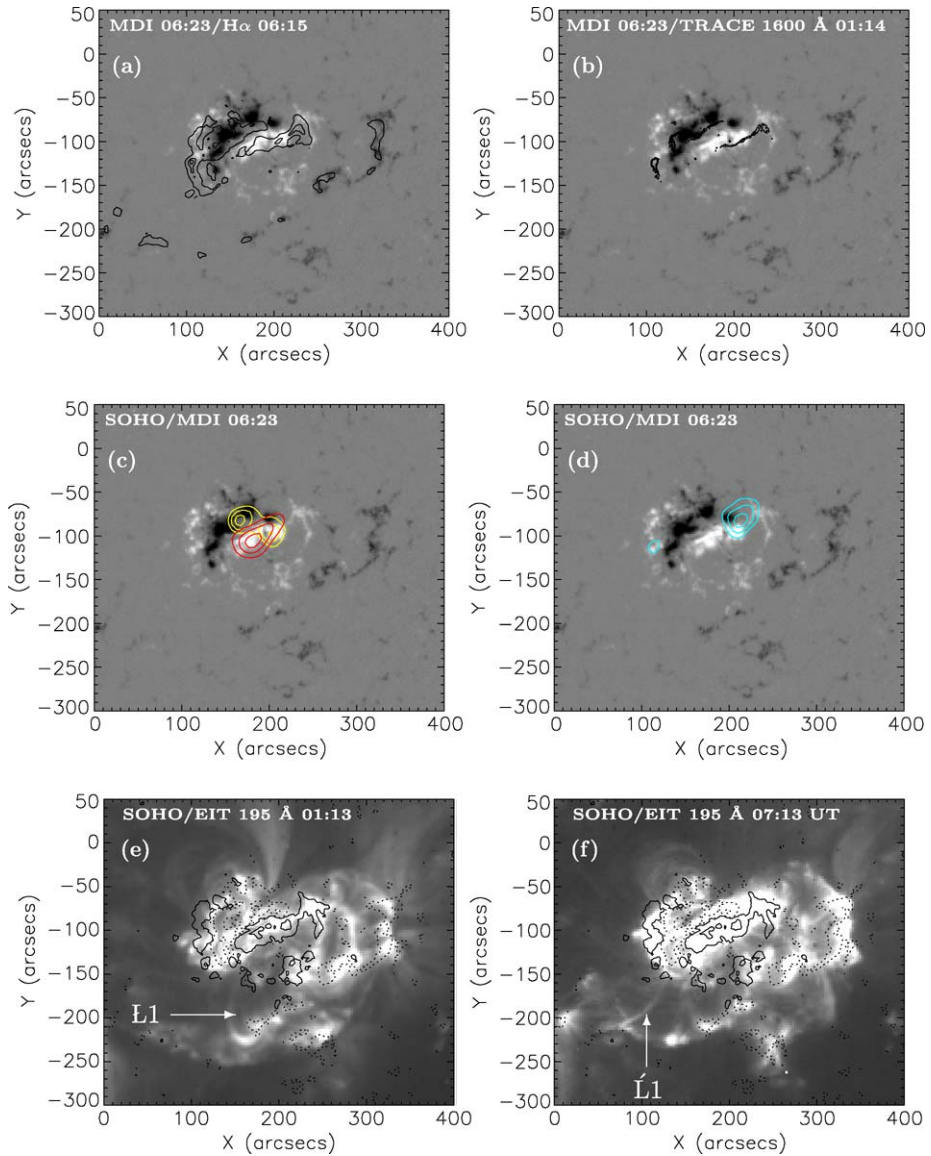


Figure 7 Co-alignment of the (a) $H\alpha$ and (b) TRACE 1600 Å ribbons with the SOHO/MDI magnetogram, MDI magnetogram overlaid by RHESSI contours (red: 6–12 keV, yellow: 25–50 keV, and cyan: 15–20 keV) during the flare (c) impulsive (06:04 UT) and (d) maximum phase (06:15 UT); contour levels are 50%, 70%, and 90% of the peak intensity. The bottom panels show SOHO/EIT images (e) before and (f) after the flare onset in 195 Å. The images are overlaid by MDI magnetogram contours (solid line: positive polarity, dotted line: negative polarity, with contour levels of ± 100 , ± 1000 , ± 1500 gauss). The loops connecting a secondary ribbon to the main flare ribbon are represented by L1 and L'1 respectively. North is up and west is to the right.

Figure 7 shows the result of the co-alignment of $H\alpha$, TRACE 1600 Å, and RHESSI HXR 15–20 keV sources with MDI magnetograms. From these figures, we can infer that

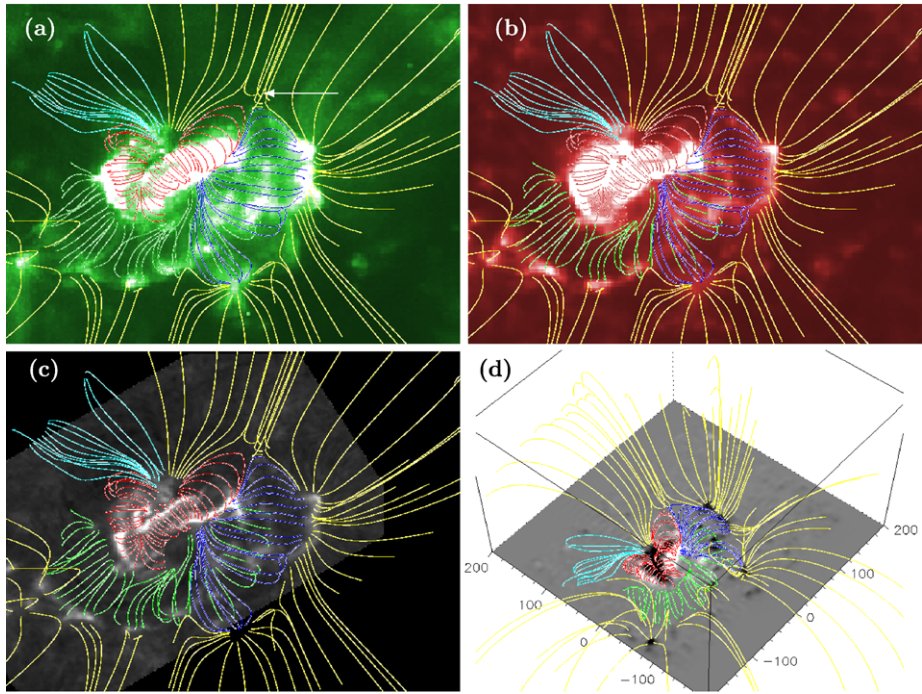


Figure 8 (a) SOHO/EIT 195 Å (07:13:30 UT), (b) SOHO/EIT 304 Å (07:19:17 UT), and (c) H α (06:15 UT) images overlaid by magnetic field lines resulting from a potential field extrapolation. (d) SOHO/MDI magnetogram at 06:24:11 UT and 3D view of magnetic field lines computed from a potential field model. The location of a null point is shown by an arrow in (a).

a strong shear is present in the flare region since the ribbon pairs R1–R2 and R3–R4 are located two-by-two in zones of opposite polarity in a nonsymmetric way. The loops associated with these ribbons are not in a potential state; otherwise their footpoints would be located symmetrically at both sides of the magnetic inversion line. The co-alignment permits us to explain the position of the ribbons, their shape, and also how their propagation is stopped where the plages have different polarities.

5. Magnetic Helicity of the Emerging Flux and Flare Ribbons

The magnetic helicity is a topological quantity that measures the torsion, the shear, and the twist of magnetic field lines in a given volume (Berger, 1984). Its definition is $H = \int \mathbf{A} \cdot \mathbf{B} d^3x$, where \mathbf{A} is the potential vector of the magnetic field \mathbf{B} .

The magnetic helicity injection has been computed for different regions by Chae, Moon, and Park (2004) and Pariat *et al.* (2006) using different methods. Recently, LaBonte, Georgoulis, and Rust (2007) carried out a statistical study relating the occurrence of big flares and found that the big flares are associated with high helicity flux. Chae, Moon, and Park (2004) present a detailed study of the rate of helicity injection in AR 10365 during its passage across the solar disk. The magnetic helicity of our region is found to be positive. The rate of helicity injection peaked on 27 May 2003, during the main activity of the active region, with the value $2.5 \times 10^{41} \text{ Mx}^2$ per hour. This is strong evidence that the emergence of

magnetic flux is an efficient process for magnetic helicity injection. The CME observed at 06:50 UT associated with this M1.6 flare very probably ejects part of this injected helicity into the heliosphere.

In Section 3 we described in detail the emerging region. The diverging flow pattern of the emerging flux (NW for $B_z < 0$ and SE for $B_z > 0$, where B_z is the normal component of the magnetic field) and the shape of the B_z patterns (especially in the $B_z > 0$ region) are both highly suggestive of magnetic “tongues” (Figure 5). The observed longitudinal magnetic field is approximately B_z because the region is close to the disk center. “Tongues” with such an orientation and evolution indicate the emergence of a flux tube with right-hand twist, that is, positive magnetic helicity, $H > 0$ (López Fuentes *et al.*, 2000). This sign corresponds to the hemispheric helicity rule discussed by Pevtsov, Canfield, and Metcalf (1995), who found that $\sim 70\%$ of southern active regions have $H > 0$, as the region studied by us.

In Section 4, we showed the flare ribbons observed in $H\alpha$ and in 1600 Å. In the central part of the region we distinguish two main forward J-shaped ribbons (Figure 5). Such a behavior has been already observed by Moore, Larosa, and Orwig (1995) and interpreted by Démoulin, Priest, and Lonie (1996). Using the concept of QSLs in 3D magnetic configurations, Démoulin *et al.* (1996, 1997) have shown that the intersection of QSLs with the chromosphere determines elongated regions that match the shape of flare ribbons. In Démoulin, Priest, and Lonie (1996), it was shown that QSLs computed in a bipolar configuration have a J shape at the chromosphere. The forward J-/reverse J-shaped ribbons indicate that the flare is triggered by coronal reconnection below a twisted flux tube of positive/negative helicity (Démoulin, Priest, and Lonie, 1996; Williams *et al.*, 2005). In our case of forward J-shaped ribbons, the twisted flux tube should have a positive helicity. Note that this QSL interpretation is also consistent with the propagation of brightenings (see Section 4.1), in the frame of slipping or slip-running reconnection (Aulanier *et al.*, 2007).

For the same event we find a good agreement between the magnetic helicity sign of the emerging flux and the signatures of reconnection in the corona (Figure 5). This kind of association was never shown before in a targeted study of a particular region. Williams *et al.* (2005) analyzed the eruption of a kink-unstable filament accompanied by a flare having J-shaped ribbons but did not describe the emergence phase of the region. The “tongue” phenomena has only been described in a few papers (Li *et al.*, 2007, Green *et al.*, 2007), but it has not been associated with flare signatures.

6. Large-Scale Magnetic Field Configuration

At the periphery of the active region 10365, secondary arc-shaped brightenings are observed at the beginning of the main flare on 27 May 2003. These secondary ribbons are visible in $H\alpha$ (R'1, R'3 in Figure 6) and in EUV (SOHO/EIT in Figure 7)

At the periphery of the active region, we observe loops in 195 Å connecting these secondary ribbons with the central part of the region and it is clear that they changed their directions during the flare [see the direction of loop L1 before the flare and the direction of loop L'1 after the flare; Figures 7(e) and 7(f)]. The secondary ribbons do not belong to the main flare; they correspond to the loops connecting relatively stable polarities of the network.

NOAA AR 10365 is highly sheared close to the main inversion magnetic line. However, at large scales in the active region we infer that the corona is in a near-potential state, as is frequently observed far from magnetic inversion lines (Schmieder *et al.*, 1996).

The $H\alpha$ and EUV secondary ribbons can be interpreted by means of a topological analysis of the coronal magnetic field above NOAA AR 10365 calculated from a lfff model

$\nabla \times \mathbf{B} = \alpha \mathbf{B}$. For simplicity, we used a potential field model, with $\alpha = 0$. This approximation is justified since we are dealing with fields that are far from the main current-carrying emerging and erupting twisted fields; the latter cannot be modeled in this approximation. Therefore we do not model the J-shaped ribbons.

Magnetic extrapolations in a potential configuration show the existence of null points, separatrices, and larger quasi-separatrix layers at high altitudes that could be responsible for the brightening of the secondary ribbons (Priest and Démoulin, 1995; Démoulin, Priest, and Lonie, 1996; Démoulin *et al.*, 1997). The lfff extrapolation method is the one used in the French Online MAGnetic Extrapolations (FROMAGE) database. It is based on the decomposition of the observed longitudinal field ($z = 0$) into harmonics using the discrete fast Fourier transform. The method was first described by Alissandrakis (1981).

Figure 8 presents the results of the extrapolation overlying the EIT 195 Å image at 07:13:30 UT, the EIT 304 Å image at 06:24:11 UT, and the MSDP H α image at 06:15 UT. All are co-aligned with the MDI magnetogram at 06:34:11 UT. The last panel represents a 3D view of the extrapolated magnetic field lines in a box smaller than the computation box, to see better the connectivities. Note that the magnetic field lines drawn in red in the central part of the region are not reliable, since this area is strongly sheared by the rotating emerging flux and the potential approximation is not appropriate, as we have already mentioned.

The magnetic field lines joining places out of the active region are drawn in yellow. These field lines are rather arbitrary because of the effects of the periodicity of the method and because of the negative flux imbalance within the active region.

The green/dark blue lines correspond to loops connecting the secondary ribbon R'1/R'3 to the eruptive area in the center of the active region. Though these loops not observed, we consider that these large-scale and weakly sheared loops must exist because of the presence of the secondary ribbons. The light blue lines are associated with ribbon R'2.

The results of the potential field extrapolation are as follows. The ribbons R'1 and R'3 visible in the EIT images and in H α (MSDP) are well explained using this approach. The lines ending in these positive polarities and going toward the periphery of the region map well to the loops directed toward the west and the south in the images of EIT/171 Å [see Figures 7(e) and 7(f) and 8(a) and 8(b)].

The pattern of field lines linked to R'2 indicates that this zone is more eruptive than we expected because numerous field lines connect to the main flare ribbons. Some blue lines are also linked to a small bright plage.

The overlying field lines indicate the possibility of the existence of a null point where some high-altitude coronal reconnection could have occurred, that is, in the zone between the red, dark blue, and the yellow lines in the north of the active region (Figure 8, arrow). Indeed, the co-alignment with the H α MSDP image shows that the secondary ribbons are located at the footpoints of the lines that come from this zone. Different scenarios could explain the triggering of this high-altitude reconnection and its manifestation as secondary remote ribbons. In case of a pre-brightening of the secondary ribbons before the flare, we could infer that we see a signature of the breakout model (Antiochos, DeVore, and Klimchuk, 1999) as observed in some events (Aulanier *et al.*, 2000; Mandrini *et al.*, 2006). In the case of brightenings occurring at the same time as the flare, these could be a remnant of an arc-shaped Moreton wave or EIT wave around the active region (Moreton, 1960; Thompson *et al.*, 1998). The brightenings observed in our case seem to be only the stationary part of the EIT waves that Delannée, Hochedez, and Aulanier (2007) explained by Joule heating at the sites of QSLs. Balasubramaniam *et al.* (2005) described the Sequential Chromospheric Brightenings (SCB) that appear to be different from the Moreton/EIT waves. They explained

these SCB as the footpoints of field lines that extend into the corona, where they are energized in sequence by magnetic reconnection as coronal fields tear from the chromosphere during the eruption.

7. Conclusion

We studied the M1.6 flare of 27 May 2003 occurring in the magnetically complex NOAA AR 10365. We used multiwavelength observations, which include different instruments: the MSDP operating in the Meudon solar tower, RHESSI, TRACE, SOHO/EIT, and SOHO/MDI.

The evolution of the photospheric magnetic configuration shows that NOAA AR 10365 is characterized by the emergence of a large, twisted magnetic flux tube. As the twisted flux is rising, diverging flows lead to a peculiar pattern of photospheric longitudinal magnetic field. The elongated polarities, positive and negative, indicate the emergence of a right-hand twisted flux tube, exhibiting two elongated “tongues” (López Fuentes *et al.*, 2000). This implies an increase of positive helicity, as also shown by Chae, Moon, and Park (2004).

In H α as well as in TRACE 1600 Å we observe a double J-shaped flare ribbons distribution. This corresponds to a positive magnetic helicity signature. The asymmetric sheared distribution of the nonthermal HXR sources observed by RHESSI in the 25–50 keV range also confirms this result. It is the first time that we have been able to find circumstantial evidence for the same sign of helicity in the flux emergence and the eruption signatures, although it has already been predicted that sunspot whorls, tongues, J-shaped ribbons, or sigmoids are signatures of magnetic helicity of the same sign according to their shape (see the review by Démoulin and Pariat, 2009).

Regarding secondary arc-shaped ribbons, observed at the periphery of the active region, we are able to correlate them with separatrices found in potential field extrapolation using the code from the database FROMAGE.

Two scenarios are possible for explaining the brightenings of the secondary ribbons: a breakout of the overlying magnetic field lines before the main flare, as Antiochos, DeVore, and Klimchuk (1999) proposed, and/or some compression and ohmic dissipation produced in separatrices during the flare, as proposed by Delannée, Hochedez, and Aulanier (2007) to explain the components of Moreton/EUV waves. Unfortunately, the lack of high-cadence observations with SOHO/EIT and the limited field of view of TRACE do not allow us to conclude whether either scenario indeed applies here. Future high-cadence and full-disk EUV images from the upcoming SDO mission should be well suited to address this issue.

Acknowledgements The authors thank Arnaud Bérurier who started the analysis of this event during a four months of training in solar physics, Dr. Pascal Démoulin for fruitful discussions, and Dr. Săm Krucker for his advice on the RHESSI data processing. We also thank the anonymous referee constructive comments and suggestions that improved the paper significantly. R.C. thanks the CEFIPRA for his postdoctoral grant. Financial support by the European Commission through the SOLAIRE Network (MTRN-CT-2006-035484) is gratefully acknowledged.

References

- Alissandrakis, C.E.: 1981, *Astron. Astrophys.* **100**, 197–200.
- Antiochos, S.K., DeVore, C.R., Klimchuk, J.A.: 1999, *Astrophys. J.* **510**, 485–493.
- Aulanier, G., DeLuca, E.E., Antiochos, S.K., McMullen, R.A., Golub, L.: 2000, *Astrophys. J.* **540**, 1126–1142.

- Aulanier, G., Golub, L., DeLuca, E.E., Cirtain, J.W., Kano, R., Lundquist, L.L., Narukage, N., Sakao, T., Weber, M.A.: 2007, *Science* **318**, 1588–1591.
- Balasubramaniam, K.S., Pevtsov, A.A., Neidig, D.F., Cliver, E.W., Thompson, B.J., Young, C.A., Martin, S.F., Kiplinger, A.: 2005, *Astrophys. J.* **630**, 1160–1167.
- Berger, M.A.: 1984, *Geophys. Astrophys. Fluid Dyn.* **30**, 79–104.
- Berlicki, A., Schmieder, B., Vilmer, N., Aulanier, G., Del Zanna, G.: 2004, *Astron. Astrophys.* **423**, 1119–1131.
- Brueckner, G.E., Howard, R.A., Koomen, M.J., Korendyke, C.M., Michels, D.J., Moses, J.D., Socker, D.G., Dere, K.P., Lamy, P.L., Llebaria, A., Bout, M.V., Schwenn, R., Simnett, G.M., Bedford, D.K., Eyles, C.J.: 1995, *Solar Phys.* **162**, 357–402.
- Chae, J., Moon, Y.J., Park, Y.D.: 2004, *Solar Phys.* **223**, 39–55.
- Chandra R., Pariat E., Schmieder B., Mandrini C.H., Uddin W.: 2009, *Solar Phys.*, submitted.
- Chen, P.F., Shibata, K.: 2000, *Astrophys. J.* **545**, 524–531.
- Choudhary, D.P., Ambastha, A., Ai, G.: 1998, *Solar Phys.* **179**, 133–140.
- Delaboudinière, J.P., Artzner, G.E., Brunaud, J., Gabriel, A.H., Hochedez, J.F., Millier, F., Song, X.Y., Au, B., Dere, K.P., Howard, R.A., Kreplin, R., Michels, D.J., Moses, J.D., Defise, J.M., Jamar, C., Rochus, P., Chauvineau, J.P., Marioge, J.P., Catura, R.C., Lemen, J.R., Shing, L., Stern, R.A., Gurman, J.B., Neupert, W.M., Maucherat, A., Clette, F., Cugnon, P., van Dessel, E.L.: 1995, *Solar Phys.* **162**, 291–312.
- Delannée, C., Hochedez, J.F., Aulanier, G.: 2007, *Astron. Astrophys.* **465**, 603–612.
- Démoulin, P.: 2007, *Adv. Space Res.* **39**, 1674–1693.
- Démoulin, P., Pariat, E.: 2009, *Adv. Space Res.* **43**, 1013–1031.
- Démoulin, P., Priest, E.R., Lonie, D.P.: 1996, *J. Geophys. Res.* **101**, 7631–7646.
- Démoulin, P., Hénoux, J.C., Priest, E.R., Mandrini, C.H.: 1996, *Astron. Astrophys.* **308**, 643–655.
- Démoulin, P., Bagala, L.G., Mandrini, C.H., Hénoux, J.C., Rovira, M.G.: 1997, *Astron. Astrophys.* **325**, 305–317.
- Green, L.M., Kliem, B., Török, T., van Driel-Gesztelyi, L., Attrill, G.D.R.: 2007, *Solar Phys.* **246**, 365–391.
- Hagyard, M.J., Venkatakrishnan, P., Smith, J.B. Jr.: 1990, *Astrophys. J. Suppl. Ser.* **73**, 159–163.
- Handy, B.N., Acton, L.W., Kankelborg, C.C., Wolfson, C.J., Akin, D.J., Bruner, M.E., Carvalho, R., Catura, R.C., Chevalier, R., Duncan, D.W., Edwards, C.G., Feinstein, C.N., Freeland, S.L., Friedlaender, F.M., Hoffmann, C.H., Hurlburt, N.E., Jurcevich, B.K., Katz, N.L., Kelly, G.A., Lemen, J.R., Levay, M., Lindgren, R.W., Mathur, D.P., Meyer, S.B., Morrison, S.J., Morrison, M.D., Nightingale, R.W., Pope, T.P., Rehse, R.A., Schrijver, C.J., Shine, R.A., Shing, L., Strong, K.T., Tarbell, T.D., Title, A.M., Torgerson, D.D., Golub, L., Bookbinder, J.A., Caldwell, D., Cheimets, P.N., Davis, W.N., Deluca, E.E., McMullen, R.A., Warren, H.P., Amato, D., Fisher, R., Maldonado, H., Parkinson, C.: 1999, *Solar Phys.* **187**, 229–260.
- Heyvaerts, J., Priest, E.R., Rust, D.M.: 1977, *Astrophys. J.* **216**, 123–137.
- Hurfurd, G.J., Schmahl, E.J., Schwartz, R.A., Conway, A.J., Aschwanden, M.J., Csillaghy, A., Dennis, B.R., Johns-Krull, C., Krucker, S., Lin, R.P., McTiernan, J., Metcalf, T.R., Sato, J., Smith, D.M.: 2002, *Solar Phys.* **210**, 61–86.
- LaBonte, B.J., Georgoulis, M.K., Rust, D.M.: 2007, *Astrophys. J.* **671**, 955–963.
- Leka, K.D., Canfield, R.C., McClymont, A.N., van Driel-Gesztelyi, L.: 1996, *Astrophys. J.* **462**, 547–560.
- Li, H., Schmieder, B., Song, M.T., Bommier, V.: 2007, *Astron. Astrophys.* **475**, 1081–1091.
- Lin, R.P., Dennis, B.R., Hurfurd, G.J., Smith, D.M., Zehnder, A., Harvey, P.R., Curtis, D.W., Pankow, D., Turin, P., Bester, M., Csillaghy, A., Lewis, M., Madden, N., van Beek, H.F., Appleby, M., Raudorf, T., McTiernan, J., Ramaty, R., Schmahl, E., Schwartz, R., Krucker, S., Abiad, R., Quinn, T., Berg, P., Hashii, M., Sterling, R., Jackson, R., Pratt, R., Campbell, R.D., Malone, D., Landis, D., Barrington-Leigh, C.P., Slassi-Sennou, S., Cork, C., Clark, D., Amato, D., Orwig, L., Boyle, R., Banks, I.S., Shirey, K., Tolbert, A.K., Zarro, D., Snow, F., Thomsen, K., Henneck, R., McHedlishvili, A., Ming, P., Fivian, M., Jordan, J., Wanner, R., Crubb, J., Preble, J., Matranga, M., Benz, A., Hudson, H., Canfield, R.C., Holman, G.D., Crannell, C., Kosugi, T., Emslie, A.G., Vilmer, N., Brown, J.C., Johns-Krull, C., Aschwanden, M., Metcalf, T., Conway, A.: 2002, *Solar Phys.* **210**, 3–32.
- López Fuentes, M.C., Démoulin, P., Mandrini, C.H., van Driel-Gesztelyi, L.: 2000, *Astrophys. J.* **544**, 540–549.
- Mandrini, C.H., Démoulin, P., Schmieder, B., Deluca, E.E., Pariat, E., Uddin, W.: 2006, *Solar Phys.* **238**, 293–312.
- Martin, S.F., Dezső, L., Antalova, A., Kucera, A., Harvey, K.L.: 1982, *Adv. Space Res.* **2**, 39–51.
- Mason, D., Komm, R., Hill, F., Howe, R., Haber, D., Hindman, B.W.: 2006, *Astrophys. J.* **645**, 1543–1553.
- Mein, P.: 1977, *Solar Phys.* **54**, 45–51.
- Mein, P.: 1991, *Astron. Astrophys.* **248**, 669–676.
- Moore, R.L., Larosa, T.N., Orwig, L.E.: 1995, *Astrophys. J.* **438**, 985–966.
- Moreton, G.E.: 1960, *Astron. J.* **65**, 494–495.

- Pariat, E., Nindos, A., Démoulin, P., Berger, M.A.: 2006, *Astron. Astrophys.* **452**, 623–630.
- Pevtsov A.A.: 2002, In: Martens, P.C.H., Cauffman, D. (eds.) *Multi-Wavelength Observations of Coronal Structure and Dynamics*, 125–134.
- Pevtsov, A.A., Canfield, R.C., Metcalf, T.R.: 1995, *Astrophys. J.* **440**, L109–L112.
- Priest, E.R., Démoulin, P.: 1995, *J. Geophys. Res.* **100**, 23443–23464.
- Roudier, T., Švanda, M., Meunier, N., Keil, S., Rieutord, M., Malherbe, J.M., Rondi, S., Molodij, G., Bommier, V., Schmieder, B.: 2008, *Astron. Astrophys.* **480**, 255–263.
- Sammis, I., Tang, F., Zirin, H.: 2000, *Astrophys. J.* **540**, 583–587.
- Scherrer, P.H., Bogart, R.S., Bush, R.I., Hoeksema, J.T., Kosovichev, A.G., Schou, J., Rosenberg, W., Springer, L., Tarbell, T.D., Title, A., Wolfson, C.J., Zayer, I., MDI Engineering Team: 1995, *Solar Phys.* **162**, 129–188.
- Schmieder, B., Démoulin, P., Aulanier, G., Golub, L.: 1996, *Astrophys. J.* **467**, 881–886.
- Schmieder, B., Hagyard, M.J., Guoxiang, A., Hongqi, Z., Kalman, B., Gyori, L., Rimpolt, B., Demoulin, P., Machado, M.E.: 1994, *Solar Phys.* **150**, 199–219.
- Schmieder, B., van Driel-Gesztelyi L.: 2005, In: Dere, K., Wang, J., Yan, Y. (eds.) *Coronal and Stellar Mass Ejections, IAU Symp.* **226**, 149–160.
- Shibata, K., Nozawa, S., Matsumoto, R.: 1992, *Pub. Astron. Soc. Japan* **44**, 265–272.
- Thompson, B.J., Plunkett, S.P., Gurman, J.B., Newmark, J.S., St. Cyr, O.C., Michels, D.J.: 1998, *Geophys. Res. Lett.* **25**, 2465–2468.
- Williams, D.R., Török, T., Démoulin, P., van Driel-Gesztelyi, L., Kliem, B.: 2005, *Astrophys. J.* **628**, L163–L166.
- Zhang, Y., Zhang, M., Zhang, H.: 2008, *Solar Phys.* **250**, 75–88.
- Zhao, J., Kosovichev, A.G.: 2004, *Astrophys. J.* **603**, 776–784.